PNAS

Supporting Information for

El Niño-Southern Oscillation forcing on carbon and water cycling in a Bornean tropical rainforest

Naoya Takamura[a,1], Yoshiaki Hata[a,1], Kazuho Matsumoto[b], Tomonori Kume[c], Masahito Ueyama[d], and Tomo'omi Kumagai[a,e,f,2]

[a] Graduate School of Agricultural and Life Sciences, The University of Tokyo, Bunkyo-ku, Tokyo 113-8657, Japan; [b] Faculty of Agriculture, University of the Ryukyus, Nishihara-cho, Okinawa 903-0213, Japan; [c] Shiiba Research Forest, Kyushu University, Shiiba-son, Miyazaki 883-0402, Japan; [d] Graduate School of Agriculture, Osaka Metropolitan University, Sakai, Osaka 599-8531, Japan; [e] Institute for Space-Earth Environmental Research, Nagoya University, Chikusa-ku, Nagoya 464-8601 Japan; [f] Water Resources Research Center, University of Hawai'i at Mānoa, Honolulu, HI 96822, USA.

[1] N.T. and Y.H. contributed equally to this work.
[2] To whom correspondence may be addressed. Email: tomoomikumagai@gmail.com

This PDF file includes:

Supporting Information Text

Inverse Big-Leaf Model for Eddy Covariance (iBLM-EC version 2.0)

In this study, we used a sun/shade model, the inverse big-leaf model for eddy covariance (iBLM-EC version 2.0; 1), coupled with photosynthesis (2) and stomatal conductance (3) submodels to invert ecosystem-scale ecophysiological traits: canopy stomatal conductance (G_c), big-leaf maximum carboxylation rate at 25°C (V_{cmax25_BL}), and Ball-Berry stomatal conductance model (3) slope (m_{BB}). Most important submodels used for our inversions are well-established, for example, the Penman-Monteith equation or the Farquhar biochemical model. Nevertheless, we describe the submodels most relevant for this analysis in the next sections for completeness. More details are available from a previous study (1).

Derivation of G_c and Meteorological Conditions on the Big-Leaf Surface

The aerodynamic conductance of sensible heat (G_b; m s^{-1}) is estimated as:

$$G_b = 1/(u/{u_*}^2 + B^{-1}/u_*), \quad [S1]$$

where

$$B^{-1} = \sum_{i=0}^{6} a_i L^i. \quad [S2]$$

In Eqs. [S1]–[S2], u and u_* (m s^{-1}) are the horizontal wind speed and friction velocity, respectively; B^{-1} is a roughness height parameter; L (m^2 m^{-2}) is the leaf area index; and a_0–a_6 are empirical constants (4) with a_0 = 8.9667, a_1 = 16.127, a_2 = −36.403, a_3 = 27.343, a_4 = −9.9967, a_5 = 1.8013, and a_6 = −0.128.

Big-leaf temperature T_c (K) is then inverted using G_b, the sensible heat flux H (W m^{-2}), and air temperature T_a (K):

$$H = c_p \rho_a G_b (T_c - T_a), \quad [S3]$$

where c_p (J kg^{-1} K^{-1}) is the specific heat of air at constant pressure and ρ_a (kg m^{-3}) is the density of dry air.

Next, G_c (mol m^{-2} s^{-1}) is calculated by applying the inverse Penman-Monteith equation to G_b, the dry canopy latent heat flux λE (W m^{-2}), and additional meteorological variables:

$${G_c}^{-1} = \left(\frac{\Delta}{\gamma}\frac{H}{\lambda E} - 1\right){G_b}^{-1} + \frac{c_p \rho_a D}{\gamma \lambda E}, \quad [S4]$$

where Δ (Pa K^{-1}) is the temperature dependence of saturation water vapor pressure, γ (Pa K^{-1}) is the psychrometric constant, and D (Pa) is the atmospheric humidity deficit above the canopy. To obtain λE, we apply the following method: first, we reject evapotranspiration measurements acquired during rainfall and within one hour after rainfall to obtain the above-dry-canopy water vapor (H_2O) flux. In-canopy radiative transfer (for incoming shortwave solar radiation (R_s) and outgoing infrared radiation) is calculated separately to estimate the net solar radiation at the soil surface (5). Potential evaporation is used to approximate soil evaporation, which is finally subtracted from the above-dry-canopy H_2O flux to obtain λE.

Several input parameters, namely u, u_*, L, H, T_a, λE, D, and R_s, can be directly derived from meteorological and eddy-covariance flux observations.

Determination of V_{cmax25_BL} and m_{BB}

Photosynthesis and Stomatal Conductance Models. The big-leaf photosynthesis rate (A; μmol m^{-2} s^{-1}), equal to gross primary productivity (GPP), is calculated with the Farquahr biochemical model (2):

$$A = \min\left(A_v,\ A_j\right) - R_{d\_BL}, \quad [S5]$$

with

$$A_v = V_{cmax\_BL}\frac{p_c - \Gamma_*}{p_c + K_c(1 + O/K_o)}, \quad [S6]$$

and

$$A_j = J_{BL}\frac{p_c - \Gamma_*}{4p_c + 8\Gamma_*}. \quad [S7]$$

The term "min(A_v, A_j)" in Eq. [S5] represents the minimum of A_v and A_j. A_v and A_j (μmol m^{-2} s^{-1}) are the gross photosynthesis rates limited by, respectively, ribulose 1,5-bisphosphate (RuBP) carboxylase-oxygenase activity and by the rate of RuBP regeneration through electron transport. R_{d_BL} (μmol m^{-2} s^{-1}) is the big-leaf daytime respiration rate excluding photorespiration. V_{cmax_BL} (μmol m^{-2} s^{-1}) is the big-leaf maximum carboxylation rate when RuBP is saturated. Within the big-leaf stomatal cavity, carbon dioxide (CO_2) partial pressure p_c (Pa) is given by $p_c = p_a C_i \times 10^{-6}$, where p_a (Pa) is the air pressure and C_i (μmol mol^{-1}) is the CO_2 concentration. Γ^* (Pa) is the CO_2 compensation point in the absence of dark respiration. K_c and K_o (Pa) are the Michaelis-Menten coefficients for CO_2 and molecular oxygen, respectively, described by the Arrhenius temperature function. O is the intercellular molecular oxygen partial pressure (approximately equal to 20,500 Pa). Finally, J_{BL} (μmol m^{-2} s^{-1}) is the big-leaf potential rate of electron transport.

The H_2O canopy stomatal conductance (G_c; mol m^{-2} s^{-1}) is related to A, to the relative humidity (h_s), and to the CO_2 concentration at the big-leaf surface (C_s; μmol mol^{-1}) by (3, 6):

$$G_c = m_{BB}\frac{Ah_s}{C_s} + b_{BB}, \quad [S8]$$

where m_{BB} and b_{BB} are the slope and the intercept of the Ball-Berry stomatal conductance model (3) obtained by linear regression analysis of data plotting G_c and Ah_s / C_s. Variables h_s and C_s can be expressed with Ohm's law if G_c and G_b are given in mol m^{-2} s^{-1}:

$$h_s = \frac{G_b e_a + G_c e_{sat}(T_c)}{G_b e_{sat}(T_c) + G_c e_{sat}(T_c)} \quad [S9]$$

and

$$C_s = \frac{G_b C_a + G_c C_i}{G_b + G_c}, \quad [S10]$$

where e_a is the atmospheric H_2O partial pressure (Pa) from meteorological observations and $e_{sat}(T_c)$ is the saturated water vapor pressure (Pa) at big-leaf temperature T_c, and C_a is the CO_2 concentration in air. To determine V_{cmax_BL} and m_{BB}, Eqs. [S5]–[S10] must be solved simultaneously with the equations defined in the next section.

Formulation of V_{cmax25_BL} and J_{BL}. The temperature dependence of V_{cmax_BL} is modeled with the Arrhenius temperature function (7):

$$V_{cmax\_BL} = V_{cmax25\_BL}\exp\left(E_a\frac{T_c - 298}{298RT_c}\right), \quad [S11]$$

where V_{cmax25_BL} is expressed in μmol m^{-2} s^{-1}, E_a (J mol^{-1}) is the activation energy, and R is the universal gas constant (R = 8.314 J mol^{-1} K^{-1}).

J_{BL} is the smaller root of the following nonrectangular hyperbola equation (7):

$$\theta_p {J_{BL}}^2 - \left(Q_e + J_{max\_BL}\right)J_{BL} + Q_e J_{max\_BL} = 0, \quad [S12]$$

with

$$Q_e = 0.5Q(1 - f), \quad [S13]$$

and

$$J_{max\_BL} = J_{max25\_BL}\frac{1+\exp\left(\frac{298S_d - E_d}{298R}\right)}{1+\exp\left(\frac{S_d T_c - E_d}{RT_c}\right)}\exp\left(E_a\frac{T_c - 298}{298RT_c}\right). \quad [S14]$$

In Eqs. [S12]–[S14], θ_p is the curvature of the big-leaf electron transport response to irradiance (θ_p = 0.7); Q and Q_e (μmol m^{-2} s^{-1}) are the photosynthetically active radiation (PAR), incoming and effectively absorbed by photosynthesis, respectively, with Q obtained by direct meteorological observation; f is the spectral correction factor (f = 0.15); J_{max_BL} and J_{max25_BL} (μmol m^{-2} s^{-1}) are the maximum value and the one at 25°C, respectively, of the big-leaf potential rate of whole-chain electron transport; S_d (J K^{-1} mol^{-1}) is an entropy term; and E_d (J mol^{-1}) is the deactivation energy.

Γ^* is expressed with a second-order polynomial (7):

$$\Gamma_* = 3.69 + 0.188(T_c - 298) + 0.0036(T_c - 298)^2. \quad [S15]$$

Like K_c, K_o and V_{cmax_BL}, R_{d_BL} is also expressed with the Arrhenius temperature function:

$$R_{d\_BL} = R_{d25\_BL}\exp\left(E_a\frac{T_c - 298}{298RT_c}\right), \quad [S16]$$

where R_{d25_BL} (μmol m^{-2} s^{-1}) is the big-leaf respiration rate at 25°C, estimated as $0.0089V_{cmax25\_BL}$.

Sun/Shade Radiative Transfer Scheme. Nominally, a big-leaf ecophysiological trait parameter X, for example, V_{cmax25_BL} or J_{max25_BL}, is expressed as the sum of the sunlit (X_{sl}) and shaded (X_{sh}) total contributions from individual leaves as:

$$X = X_{sl} + X_{sh} = x_0 L_{sl} + X_{sh}, \quad [S17]$$

where x_0 is the individual leaf ecophysiological trait and L_{sl} is the leaf area index for sunlit leaves. Assuming similar vertical distributions for irradiance and leaf nitrogen, x_0 is then calculated by solving the following equations:

$$X_{sl} = X \frac{k_n \Omega}{k_n + k_b \Omega L} \frac{1 - \exp[-(k_n + k_b \Omega L)]}{1 - \exp(-k_n)}, \quad [S18]$$

$$L_{sl} = \frac{1 - \exp(-k_b \Omega L)}{k_b}, \quad [S19]$$

$$x_0 = \frac{X_{sl}}{L_{sl}}, \quad [S20]$$

$$\ln(k_n) = 0.00963 v_{cmax25} - 2.43, \quad [S21]$$

where k_n is the nitrogen extinction coefficient related to the individual leaf maximum carboxylation rate at 25°C (v_{cmax25}; μmol m^{-2} s^{-1}; 8), and Ω is the clumping factor (Ω = 0.66; 9).
The beam extinction coefficient k_b is given by (10):

$$k_b = \frac{G(\omega)}{\cos \omega}, \quad [S22]$$

where ω is the solar zenith angle. G is the projection of the total leaf area within a given layer onto a plane normal to the direction ω of the leaves. It is obtained from look-up tables as a function of ω by assuming a spherical, planophile, or erectophile leaf angle distribution (11).

Optimization. Final values of the big-leaf photosynthesis and stomatal conductance model parameters V_{cmax25_BL}, $J_{max25\_BL}/V_{cmax25\_BL}$, m_{BB}, and b_{BB} were determined with the shuffled complex evolution method, a global optimization algorithm developed at the University of Arizona (SCE-UA; 12–14). Optimization was applied to half-hourly GPP and λE data with a seven-day moving window. Initial input parameter ranges were set to 0.1–700 μmol m^{-2} s^{-1} for V_{cmax25_BL}, 1.8–2.7 for $J_{max25\_BL}/V_{cmax25\_BL}$ (15–17), 0.1–100 for m_{BB}, and 0–1 mmol m^{-2} s^{-1} for b_{BB}. Applying the moving window to seasonally varying parameters allowed the model to account for changes in ecophysiological traits, such as periodic or sporadic drought stress.

During the optimization process, uncertainty ranges for m_{BB} and b_{BB} were first initialized to the standard deviations of a set of ten optimized values calculated from randomly selected initial values. Then, V_{cmax25_BL}, $J_{max25\_BL}/V_{cmax25\_BL}$, m_{BB}, and b_{BB} were determined by minimizing the root-mean-square error between observed and modeled transpiration data, with observed GPP tentatively used in Eq. [S8] as an estimate of A. Eq. [S8] was subsequently coupled with the derivatives of Eqs. [S9] and [S10] calculated on the basis of Fick's law, inducing a strong observational constraint on m_{BB} and b_{BB}. Finally, m_{BB} and b_{BB} were recalculated for the range determined during the first iteration on λE.

Because ten iterations were sufficient to converge towards global optima (18), parameter uncertainty ranges were derived from ten optimized values calculated from randomly selected initial values. Optimized parameters were used for subsequent calculations only if the calculated uncertainty was less than 10% of their absolute value. Therefore, the final estimated uncertainties on the optimized parameters were less than 10%.

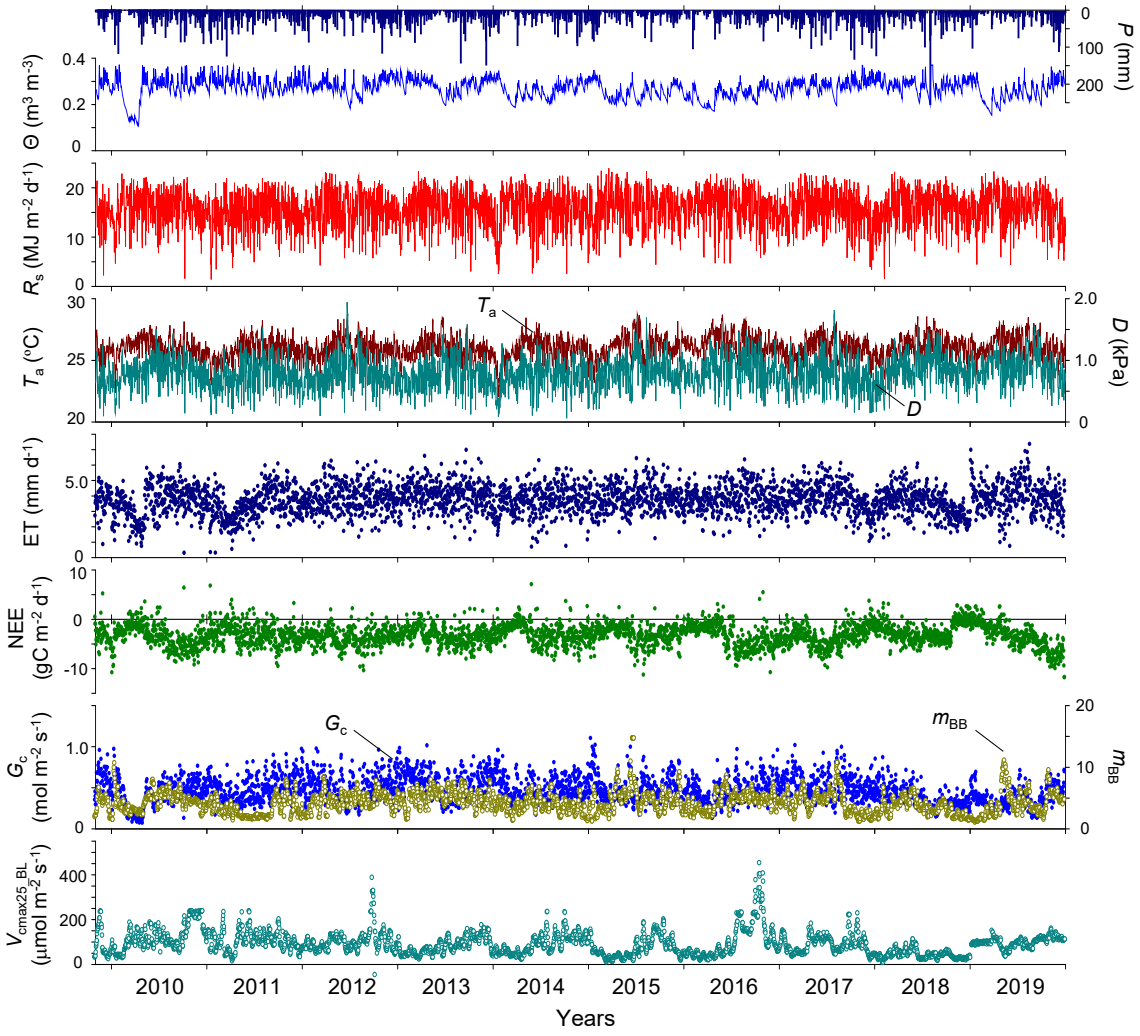

Fig. S1. Time series of meteorological variables, canopy exchange properties, and ecophysiological traits over the study period (late 2009–2019). From top to bottom: daily total precipitation (P), volumetric soil moisture content in the 0–50 cm soil layer (Θ), daily total incoming solar radiation (R_s), daily mean air temperature (T_a) and mean daytime atmospheric humidity deficit (D), daily evapotranspiration (ET), daily net ecosystem exchange (NEE), mean daytime canopy conductance (G_c) and Ball-Berry model slope (m_{BB}), and big-leaf maximum carboxylation rate at 25°C (V_{cmax25_BL}).

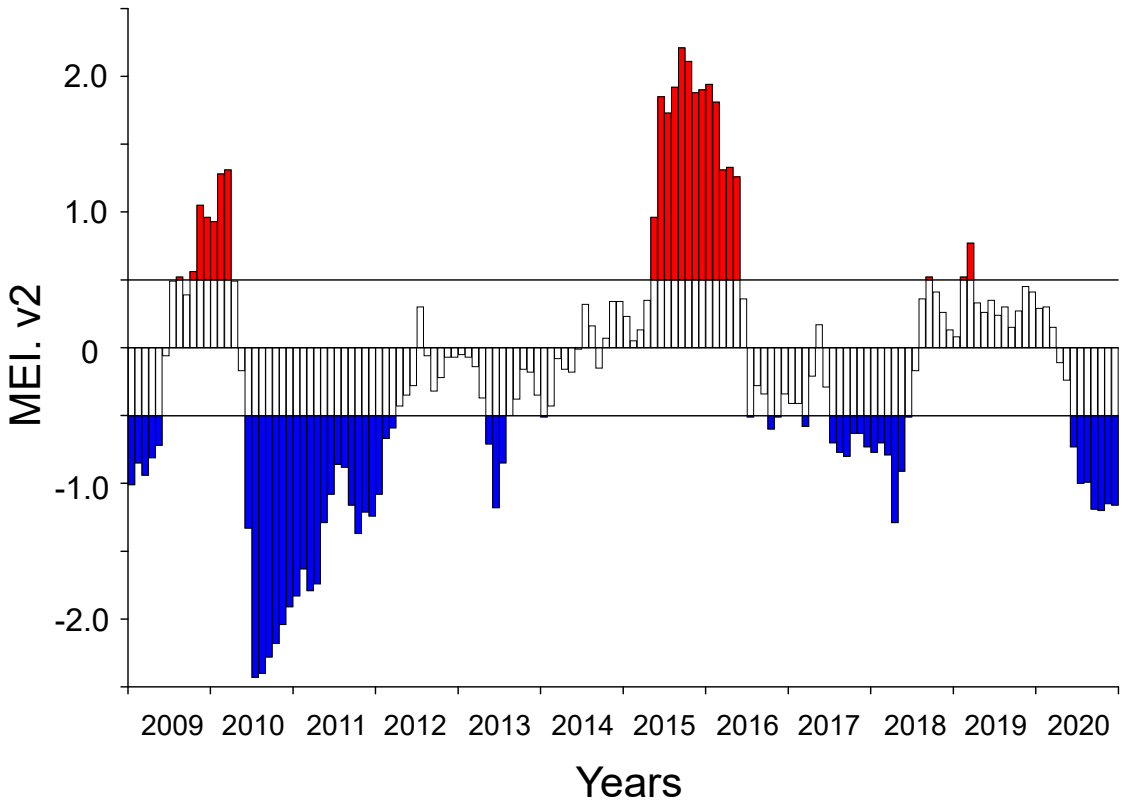

Fig. S2. Monthly multivariate El Niño-Southern Oscillation (ENSO) index (MEI.v2, retrieved from https://psl.noaa.gov/enso/mei/). Upper and lower horizontal lines represent thresholds of +0.5 and −0.5, respectively. Red and blue bars indicate El Niño (months with MEI > +0.5) and La Niña (months with MEI < −0.5) conditions, respectively.

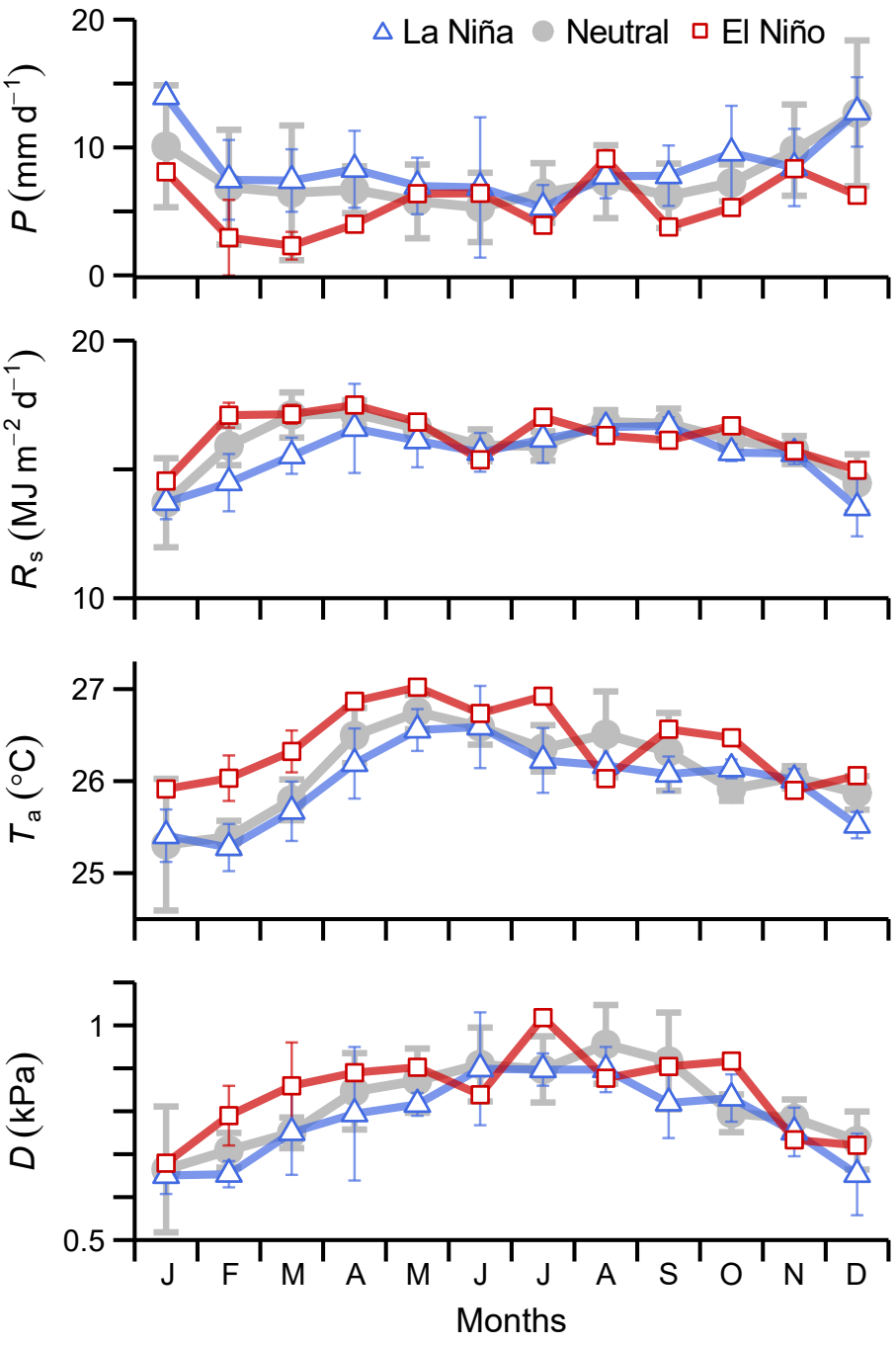

Fig. S3. Annual variations of meteorological variables in the La Niña (blue curve and triangles), neutral (grey curve and filled circles), and El Niño (red curve and squares) phases over the study period. From top to bottom, monthly mean values are plotted for P, R_s, T_a, and D. Vertical bars represent plus or minus one standard deviation around the mean for numbers higher than three.

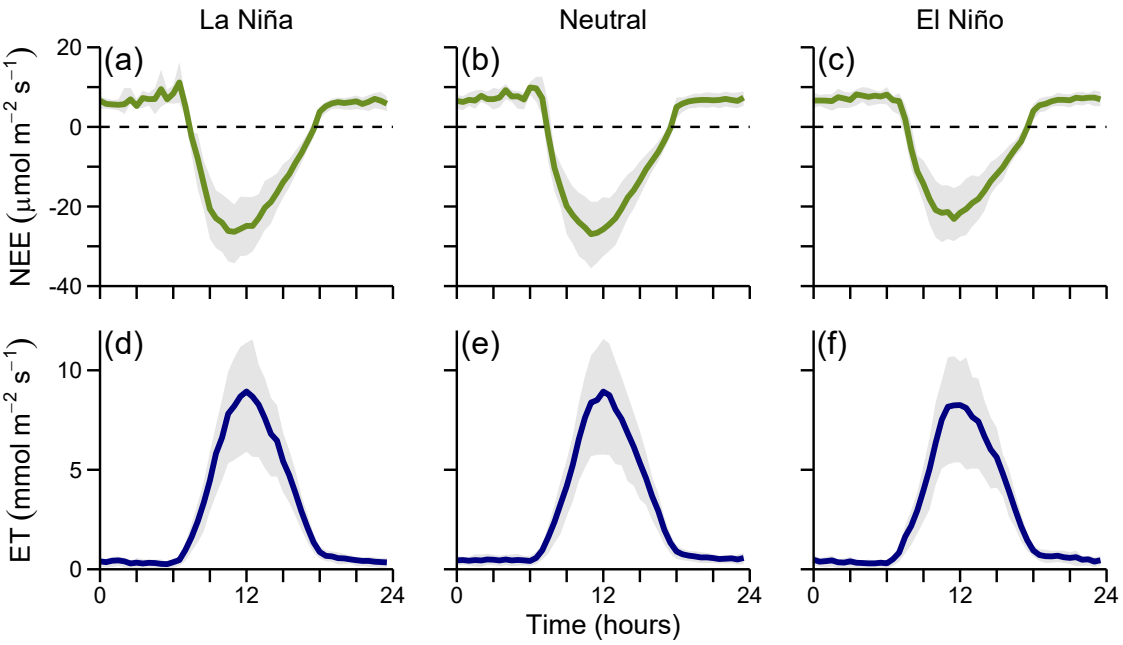

Fig. S4. Mean diurnal variations of (a–c) mean NEE and (d–f) ET in the La Niña (left; Panels a, d), neutral (center; Panels b, e), and El Niño (right; Panels c, f) phases. The lower and upper boundaries of the shaded area indicate the first and third quartiles, respectively, of the observation data in each ENSO phase. Only eddy-covariance flux data classified as “measured” (quality control flag of 0; 19) were selected.

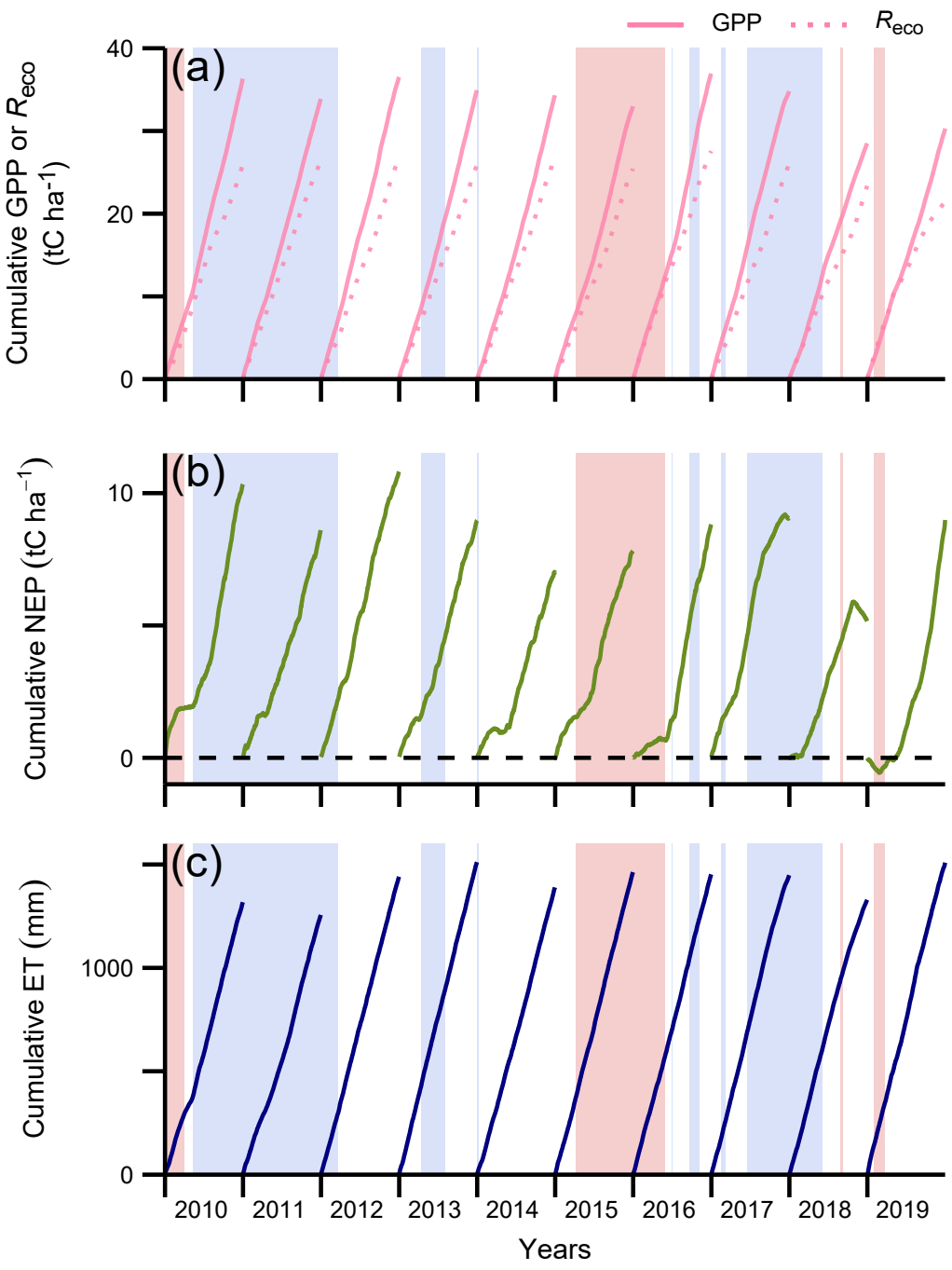

Fig. S5. Interannual variations of the carbon balance (a, b) and cumulative ET (c). The carbon balance is evaluated from gross primary productivity (GPP), ecosystem respiration (R_{eco}), and net ecosystem productivity (NEP) as their cumulative values. Red and blue shadings identify El Niño and La Niña events, respectively.

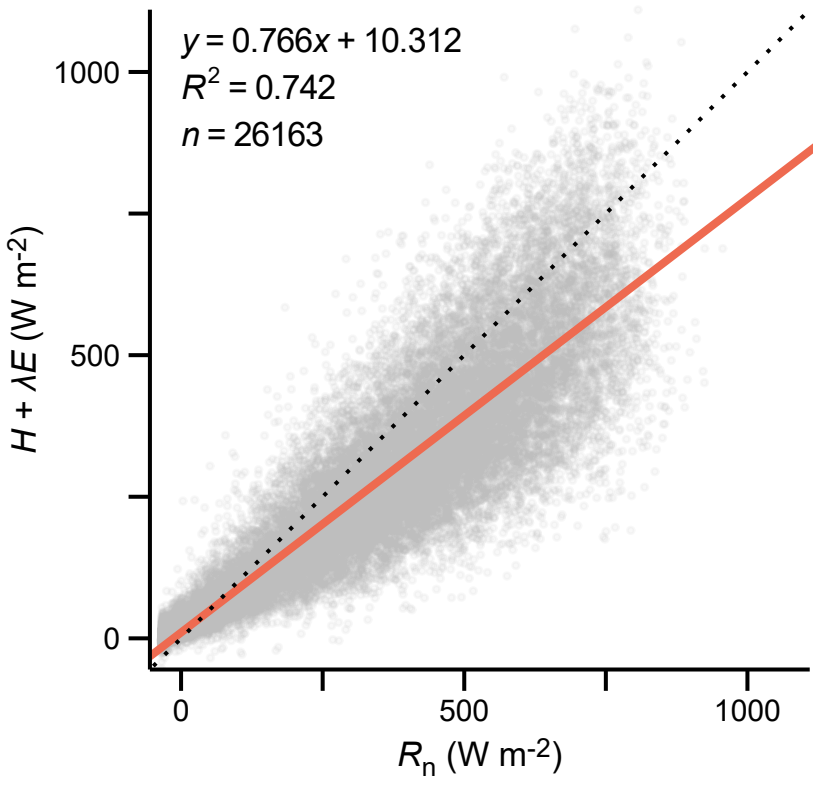

Fig. S6. Energy balance at the studied forest stand over the study period. The sum of the observed sensible and latent energy fluxes ($H + \lambda E$; vertical axis) is plotted as a function of the net radiation (R_n; horizontal axis). The linear regression (thick line) model, the Pearson's correlation coefficient value, and the number of independent data points are given in the top left corner. The 1:1 curve (dotted line) is also shown. Only data acquired during daylight hours were selected.

SI References

1. M. Ueyama, *et al.*, Inferring CO_2 fertilization effect based on global monitoring land-atmosphere exchange with a theoretical model. *Environmental Research Letters* **15**, 084009 (2020).
2. G. D. Farquhar, S. von Caemmerer, J. A. Berry, A biochemical model of photosynthetic CO_2 assimilation in leaves of C_3 species. *Planta* **149**, 78–90 (1980).
3. G. J. Collatz, J. T. Ball, C. Grivet, J. A. Berry, Physiological and environmental regulation of stomatal conductance, photosynthesis and transpiration: a model that includes a laminar boundary layer. *Agricultural and Forest Meteorology* **54**, 107–136 (1991).
4. J.-P. Lhomme, A. Chehbouni, B. Monteny, Sensible heat flux-radiometric surface temperature relationship over sparse vegetation: Parameterizing B-1. *Boundary-Layer Meteorology* **97**, 431–457 (2000).
5. Y. Ryu, *et al.*, Integration of MODIS land and atmosphere products with a coupled-process model to estimate gross primary productivity and evapotranspiration from 1 km to global scales. *Global Biogeochemical Cycles* **25** (2011).
6. J. T. Ball, I. E. Woodrow, J. A. Berry, "A model predicting stomatal conductance and its contribution to the control of photosynthesis under different environmental conditions" in *Progress in Photosynthesis Research*, (Springer, 1987), pp. 221–224.
7. D. G. G. de Pury, G. D. Farquhar, Simple scaling of photosynthesis from leaves to canopies without the errors of big-leaf models. *Plant, Cell & Environment* **20**, 537–557 (1997).
8. J. Lloyd, *et al.*, Optimisation of photosynthetic carbon gain and within-canopy gradients of associated foliar traits for Amazon forest trees. *Biogeosciences* **7**, 1833–1859 (2010).
9. L. He, J. M. Chen, J. Pisek, C. B. Schaaf, A. H. Strahler, Global clumping index map derived from the MODIS BRDF product. *Remote Sensing of Environment* **119**, 118–130 (2012).
10. J. Goudriaan, *Crop micrometeorology: a simulation study* (Wageningen University and Research, 1977).
11. J. Pisek, O. Sonnentag, A. D. Richardson, M. Mõttus, Is the spherical leaf inclination angle distribution a valid assumption for temperate and boreal broadleaf tree species? *Agricultural and Forest Meteorology* **169**, 186–194 (2013).
12. Q. Y. Duan, V. K. Gupta, S. Sorooshian, Shuffled complex evolution approach for effective and efficient global minimization. *Journal of Optimization Theory and Applications* **76**, 501–521 (1993).
13. Q. Duan, S. Sorooshian, V. Gupta, Effective and efficient global optimization for conceptual rainfall-runoff models. *Water Resources Research* **28**, 1015–1031 (1992).
14. Q. Duan, S. Sorooshian, V. K. Gupta, Optimal use of the SCE-UA global optimization method for calibrating watershed models. *Journal of Hydrology* **158**, 265–284 (1994).
15. S. von Caemmerer, G. Farquhar, J. Berry, "Biochemical model of C_3 photosynthesis" in *Photosynthesis*, (Springer, 2009), pp. 209–230.
16. Y. P. Wang, D. Baldocchi, R. A. Y. Leuning, E. V. A. Falge, T. Vesala, Estimating parameters in a land-surface model by applying nonlinear inversion to eddy covariance flux measurements from eight Fluxnet sites. *Global Change Biology* **13**, 652–670 (2007).
17. S. D. Wullschleger, Biochemical limitations to carbon assimilation in C_3 plants—a retrospective analysis of the A/C_i curves from 109 species. *Journal of Experimental Botany* **44**, 907–920 (1993).
18. M. Ueyama, *et al.*, Optimization of a biochemical model with eddy covariance measurements in black spruce forests of Alaska for estimating CO_2 fertilization effects. *Agricultural and Forest Meteorology* **222**, 98–111 (2016).
19. G. Pastorello, *et al.*, The FLUXNET2015 dataset and the ONEFlux processing pipeline for eddy covariance data. *Scientific Data* **7**, 1–27 (2020).